Multi-antenna based One-Bit Spatio-Temporal Wideband Sensing for Cognitive Radio Networks

J.C. Merlano-Duncan[+], Shree Krishna Sharma[†], Symeon Chatzinotas[+], Björn Ottersten[+], Xianbin Wang[†]

SnT - securityandtrust.lu, University of Luxembourg, Luxembourg[+]
University of Western Ontario, London, Canada[†]
Email: {juan.duncan, symeon.chatzinotas, bjorn.ottersten}@uni.lu,
{sshar323, xianbin.wang}@uwo.ca

***Abstract*— Cognitive Radio (CR) communication has been considered as one of the promising technologies to enable dynamic spectrum sharing in the next generation of wireless networks. Among several possible enabling techniques, Spectrum Sensing (SS) is one of the key aspects for enabling opportunistic spectrum access in CR Networks (CRN). From practical perspectives, it is important to design low-complexity wideband CR receiver having low resolution Analog to Digital Converter (ADC) working at a reasonable sampling rate. In this context, this paper proposes a novel spatio-temporal wideband SS technique by employing multiple antennas and one-bit quantization at the CR node, which subsequently enables the use of a reasonable sampling rate. In our analysis, we show that for the same sensing performance requirements, the proposed wideband receiver can have lower power consumption than the conventional CR receiver equipped with a single-antenna and a high-resolution ADC. Furthermore, the proposed technique exploits the spatial dimension by estimating the direction of arrival of Primary User (PU) signals, which is not possible by the conventional SS methods and can be of a significant benefit in a CRN. Moreover, we evaluate the performance of the proposed technique and analyze the effects of one-bit quantization with the help of numerical results.**

I. Introduction

One of the main challenges towards meeting the capacity requirements of the Fifth Generation (5G) wireless Communications is the lack of usable radio spectrum [1]. In this regard, several promising solutions such as dynamic spectrum sharing, exploitation of unlicensed WiFi spectrum, and licensed shared access mechanisms are under investigation [1], [2]. Towards enabling dynamic spectrum sharing among heterogeneous wireless networks, Cognitive Radio (CR) communication can exploit the available radio resources in a flexible and intelligent manner with the help of various spectrum awareness and exploitation techniques [3], [4]. In a CR Network (CRN), the cognitive devices, which are named as Secondary Users (SUs), must be aware of their surroundings and occupy the available spots of the radio frequency spectrum that are not used by the licensed Primary Users (PUs) at a particular location and time.

Spectrum Sensing (SS) is one of the main functionalities required by a CR and in most of the cases, it requires the estimation of the receiver noise in an explicit or implicit way in order to perform accurate signal detection. However, in a practical scenario, the receiver noise can not be perfectly known (i.e., noise variance uncertainty phenomena), which gives as a consequence the existence of Signal to Noise Ratio (SNR) walls [5], [6], which are the limits in the negative values of the SNR beyond which it is impossible to have an accurate detection even if the sensing is performed during unlimited periods [5], [6]. Towards addressing this problem, Generalized Energy Detector (GED) has been recently proposed as a promising solution [7], [8]. Although there are other alternatives such as eigenvalue based detector and the cyclostationary feature detector [4], these techniques require a much higher level of detector complexity as compared to the GED.

In the GED, it is assumed that when a wideband spectrum is simultaneously sensed, there is at least one empty subband which can be used to perform detection over the other subbands using a ratio-based test statistic. However, if the sensing time is increased, the probability of getting at least one empty subband decreases, which becomes an issue for the GED technique. Also, the accuracy of the conventional GED depends implicitly on the ergodicity of the noise process at the receiver. Therefore, if the noise power changes over time, as it is commonly observed in practical scenarios, the increase of the sensing time may result in the degradation of the detection performance. Another drawback of the existing techniques including the GED is that they do not provide any spatial information about the interfering PU signals, although acquiring and using this information can significantly improve the performance of the CRN.

In order to address the aforementioned drawbacks of the GED, we propose a novel technique based on a muti-antenna receiver with one-bit quantization in the Analog to Digital Converter (ADC), which can reduce the required sensing time considerably while keeping reasonable system complexity and power consumption. The proposed technique can be applied in 5G massive Multiple Input Multiple Output (MIMO) base stations, in which the number of antennas is increased at least one or two orders of magnitude [9]. The power consumption and the cost of a digital radio receiver are mostly determined by the Radio Frequency (RF) front-end and the ADC. The power consumed by these two elements increases as the amplitude (and therefore the SNR) of the received signals is increased. In addition, in order to achieve the high SNR after quantization, the number of quantization bits is increased

978-1-4673-8999-0/17/$31.00 ©2017 IEEE

resulting in a considerable increase in power consumption and system complexity. As an instance, one of the most popular ADC technologies used in wireless communications, the flash topology, follows a model in which the power consumption and chip size are increased exponentially with the number of bits and linearly with the sampling frequency [10], and a typical commercially available high resolution ADC has a power consumption of several Watts.

Towards reducing the power consumption, the use of one bit quantization has been previously investigated for communication and channel estimation purposes [11], [12]. In [13], an SS method for CR applications using one-bit ADC has been proposed, and it has been shown that the feasibility of the detector depends on the increase of the sampling frequency in a few orders of magnitude, thus resulting in higher power consumption. Also, the use of few number of bits for spectrum sensing has been proposed in [14], [15], where the use of a fusion center is proposed which performs Mean Square Error (MSE) or Maximum Likelihood (ML) estimations using few-bits quantized signals generated by scattered low-end sensors. In contrast to the aforementioned works, this paper examines the possibility of employing multiple antennas to enable the use of one-bit ADC with reasonable sampling rate in a CRN. We propose the use of a multi-antenna compact station, which is a synchronized array that performs coherent beamforming at its reception. This allows to meet stringent low SNR requirements while maintaining the total consumed power and the total system complexity in the same order of magnitude as that of the single antenna case. Besides, in the proposed scheme, the SU can detect the PU signals in different frequency subbands, and in addition, can find their directions of arrival, which can be subsequently utilized to employ suitable interference mitigation techniques at the SU in order to provide better protection to the PU receivers.

In this paper, first, we propose a spatio-temporal acquisition model using a two-dimensional (2D) planar array. Subsequently, we propose the use of one-bit (per complex element, I and Q) quantization of the baseband down-converted signal. The acquired samples are used to obtain a tri-dimensional Power Spectrum Density (PSD) map of the received signal during a sensing period. This map is then classified using an edge detection algorithm in several sub-sets, which are evaluated as occupied or not using the GED detector. We show that with the proposed technique, the total power consumption and system complexity can be decreased while increasing the detection performance compared to the single-antenna high-resolution ADC case. Finally, we evaluate the performance of the proposed technique and analyze the effects of one-bit quantization with the help of numerical results.

The remainder of this paper is organized as follows: In Section II, the system model and problem statement are described. In Section III, the proposed multi-dimensional wideband SS technique is presented. Numerical results are provided in Section IV. Finally, Section V concludes the paper.

II. System Model and Problem Statement

Let us consider an SU which needs to perform SS over a wide range of frequencies which have different PSDs and come from different incident directions. We assume that the SU attempts to identify and perform sensing for each sub-band and utilizes only white sub-bands for communications.

For the analysis of the detector performance, it is observed that a given PSD is associated to a unique surface power density flux (measured in Watts/Hz/m^2). This flux can be derived from the regulations reports (Federal Communications Commission [FCC], Electronic Communications Committee [ECC] and others), where they also assume an omnidirectional antenna in the receiver [16], [17]. As an example, it is stated in FCC recommendations that in order to provide an acceptable level of protection to the primary network, the SU should be able to detect signals with a total power of -120dBm integrated inside a TV band, which is 6MHz [16], [17]. This should be done with the maximum sensing time of 2 seconds, and assuming that the SU uses a non-directive antenna with 0dBi gain. Having the receiver at ambient temperature and with an estimate for the noise figure of 6dB, which can be seen as very benign estimate[1], it will represent an SNR of -20dB. These signals can not be accurately detected by a conventional energy detector due to the SNR wall effect [5], [7], [8].

A. Antenna array analysis

The proposed cognitive device is equipped with N antennas, distributed over a 2D surface to perform the signal acquisition. The set of antennas is equally spaced in the $\mathbf{x}$ and $\mathbf{y}$ axes and each of them is located at a position in the $[x, y]$ plane. Figure 1 shows one receiving antenna of the planar array which is impinged by an incident wavefront which comes at the angles θ and ϕ. A given incident wavefront will produce a signal $S_{0w}(t)$ as a function of time at an antenna located in $x = 0$, $y = 0$.

The signal back-propagated to the position $[x, y]$, by the same wavefront can be obtained from the geometry of Figure 1 to be [18]

$$S_w(t, x, y) = S_{0w}(t) e^{j2\pi(x \sin\theta \cos\phi + y \sin\theta \sin\phi)}, \quad (1)$$

given that the source is far enough from the 2D surface that both positions receive the wavefront with the same incident angle. Assuming that the intensity of the incident wavefront as a function of the incident angle is $v(t, \theta, \phi)$, the total signal collected by an antenna located at $[x, y]$, will be integral of all the incident waveforms which is given by [18]

$$V(t, x, y) = \int_0^{2\pi} \int_0^{\pi} v(t, \theta, \phi)\, G(\theta, \phi) \quad \cdot \\ e^{j2\pi(x \sin\theta \cos\phi + y \sin\theta \sin\phi)} \sin\theta d\theta d\phi. \quad (2)$$

We assume that the receiving antennas have a gain $G(\theta, \phi)$ expressed as a function of the incident solid angle $[\theta, \phi]$ with respect to the 2D surface. In our case, we assume for

[1]Estimate of the noise figure of the entire receive chain, from amplifiers to ADC.

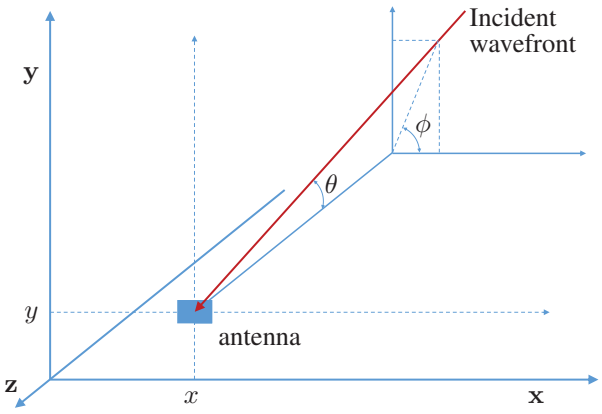

Fig. 1. Receiving geometry for one antenna within the 2D array. The angles θ and ϕ are taken with respect to the projection on the x and y reference planes [18].

simplicity that $G(\theta, \phi)$ has a constant value $G_0(\theta, \phi)$ for $[\theta, \phi]$ in the range $([0, \pi/2], [0, 2\pi])$ and zero outside this range. This represents a 3dBi gain given by a half-sphere radiation pattern. From this, an estimation of the intensity function can be obtained from the inverse Fourier transform of the $V(t, x, y)$ measurements by [18]

$$\tilde{v}(t, \eta, \zeta) = \int_{-\infty}^{\infty} \int_{-\infty}^{\infty} V(t, x, y) \cdot e^{-j2\pi(x \sin\theta \cos\phi + y \sin\theta \sin\phi)} dxdy. \quad (3)$$

The above expression is well known in the interferometric radiometry community [18]–[20]. It can be expressed in terms of the angular frequency variables $(\zeta, \eta) = (\sin\theta \cos\phi, \sin\theta \sin\phi)$, as

$$\tilde{v}(t, \eta, \zeta) = \int_{-\infty}^{\infty} \int_{-\infty}^{\infty} V(t, x_i, y_i) e^{-j2\pi(x\zeta + y\eta)} dxdy. \quad (4)$$

We introduce $\tilde{v}_\omega(f, \eta, \zeta)$, which is the Fourier transform in the t variable of $\tilde{v}_0(t, \eta, \zeta)$ by

$$\tilde{v}_\omega(f, \eta, \zeta) = \int_{-\infty}^{\infty} \tilde{v}(t, \eta, \zeta) e^{-j2\pi ft}\, dt = \int_{-\infty}^{\infty} \int_{-\infty}^{\infty} \int_{-\infty}^{\infty} V(t, x, y) e^{-j2\pi(x\zeta + y\eta + ft)} dxdydt, \quad (5)$$

which is an estimation of the radiation intensity as a function of the temporal and angular frequencies. However, in a practical application scenario, the acquired signal is restricted by a number of finite samples in time and space using an array with a finite number of antennas, as shown in Figure 2. Here, we determine a given number of rows and columns in the 2D plane, N_x and N_y. For this, the SU collects a finite number of time samples N_t acquired by each antenna to have a discrete version of $V(t, x, y)$ over a finite interval.

The signal received by the antenna array, at a given discrete time i at each antenna (row n, and column m) will be

$$s(i, n, m) = V(i\Delta_t, n\Delta_d, m\Delta_d), \; i = 1, ..., N_t, \; n = 1, ..., N_x, \; m = 1, ..., N_y. \quad (6)$$

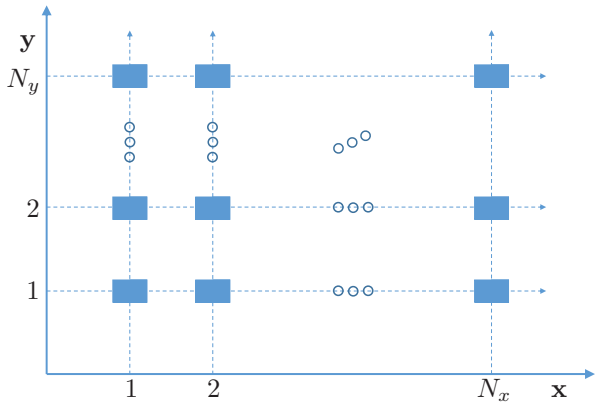

Fig. 2. Receiving array geometry. The antennas have a constant separation for the indexes of x and y.

Using $s(i, n, m)$, we can have a discrete version of $\tilde{v}_\omega(f, \eta, \zeta)$ where the integrals of the equation can be replaced by a summation of discrete samples, to have a Discrete Fourier Transform, defined by

$$D_\omega(k_t, k_x, k_y) = \sum_{i=0}^{N_t-1} \sum_{m=0}^{N_y-1} \sum_{n=0}^{N_x-1} \frac{s(i, n, m)\, e^{-\frac{j2\pi(ik_t + nk_x + mk_y)}{N_t N_x N_y}}}{\sqrt{N_t N_x N_y}}, \; k_t = 1, ..., N_t, \; k_x = 1, ..., N_x, \; k_y = 1, ..., N_y. \quad (7)$$

B. Receiver signal model

We assume that the incident wavefront from a single PU is observed as coming at a unique incident angle for all the receiving antennas in the SU array. The complex sampled baseband signal at the receiver after down-conversion and filtering becomes

$$\tilde{s}(i, m, n) = s(i, m, n) + w(i, m, n), \quad (8)$$

where the elements of $w(i, m, n) \backsim C\mathfrak{N}(0, \sigma^2) \forall (i, m, n)$ are independent and identically distributed zero mean circularly symmetric complex Gaussian (ZMCSCG) random variables, all with unknown variance σ^2, generated by the antenna temperature, antenna temperature efficiency and the noise figure of the the receiver chains. It is assumed that the PU signal has a wide-band Gaussian distribution, with a surface power spectrum density flux measured in Watts/Hz/m^2, which is almost constant within the subband which is at least B_{min}Hz. However, in the following we are not assuming

that the primary signals do not generate tail-shaped out-of-band interferences to the adjacent subbands. The total scanned bandwidth is assumed to have one or more white sub-bands as in [7]. These assumptions are reasonable since according to the FCC report, spectrum utilization in most frequency bands can be quite low [16], [17]. Here, we assume that all the antennas are at the same temperature for a given acquisition and this temperature does not vary during the acquisition, and all the receiver chains have the same noise figure. Consequently, it is assumed that all the receivers have the same noise variance during one acquisition.

III. Multi-Dimensional Wideband Sensing

In order to perform SS at the SU, the baseband signals are quantized using one-bit ADCs. Therefore, the sign of the I and Q components of the baseband signal $\tilde{s}(i,m,n)$ is quantized in the following way

$$\tilde{s}_q(i,m,n) = \text{sign}(\text{real}(\tilde{s}(i,m,n))) + j\text{sign}(\text{imag}(\tilde{s}(i,m,n))). \tag{9}$$

Then, the transformation for the quantized signals becomes

$$D_{\omega q}(k_t,k_x,k_y) = \sum_{i=0}^{N_t-1}\sum_{m=0}^{N_y-1}\sum_{n=0}^{N_x-1}\frac{\tilde{s}_q(i,n,m)\; e^{-\frac{j2\pi(ik_t+nk_x+mk_y)}{N_tN_xN_y}}}{\sqrt{N_tN_xN_y}}, \quad \begin{matrix} k_t=1,...,N_t, \\ k_x=1,...,N_x, \\ k_y=1,...,N_y. \end{matrix} \tag{10}$$

Subsequently, this signal is used to get the test statistics required by the SU.

In this paper, we propose to employ the Generalized Energy Detector (GED) proposed in [7] and [8] for the detection of the white subbands, however, in this case, the procedure is applied to the tridimensional array $D_{\omega q}(k_t,k_x,k_y)$, which includes two axes for the angular frequency, and one axis for the temporal frequency. The procedure is described as follows

- Detect the boundaries of the subbands in frequencies (two angular axes and one temporal axes). For this, a new method based on the edge detection procedure [7] is used.
- Detect the subband (in temporal and angular frequencies) with minimum power spectrum density and use it as the reference subband for the detection of the rest of subbands [7].
- Perform subband detection using the GED computing the ratio of the average PSD of the evaluated subbands to the PSD of reference subband.

In the following subsections, these three steps are discussed. Additionally, the quantization effects of the one-bit ADC are taken into consideration. It is worth to mention that in [11] and [12], it has been shown that the effect of one-bit quantization goes to a limit of $2/\pi$ of degradation in achievable channel capacity as the input SNR goes low [11], [12]. In our work, we found by mean of simulations that the degradation of the ratio-based test statistic approaches to the $2/\pi$ limit as the incident SNR goes to low values.

A. Edge Detection

It is required to detect the boundaries of the subbands and classify different volumetric spaces in order to perform the GED in each of the subbands. In this case, the detection of the edges in the temporal frequency domain is similar to the one described in [7] for each of the vectors associated to one pair of points k_x, k_y. For this operation, one or more realizations of $D_{\omega q}(k_t,k_x,k_y)$ can be used. After this, the final operation to classify the subbands is to detect the boundaries in the angular frequency axes.

For the detection of the boundaries in the k_t axis, we assume a minimum detectable size for any subband, which is denoted by B_{min} (Hz). Using one single realization of $D_{\omega q}$, it is possible to obtain a test statistic that can indicate the presence of an edge in point k_{t0} over the k_t axis for a given k_x, k_y point. The test statistics are obtained from the ratio of the average of the magnitude squared of $D_{\omega q}$ at the left and right sides of k_t over N_{et} number of samples $N_{et} = \lfloor \frac{B_{\text{min}}T}{2} \rfloor$, where T is the sampling time period. Therefore, the test statistics becomes

$$R_{et}(k_{t0}) = \sqrt{\frac{N_{et}}{2}}\left(\frac{\sum_{k_t=k_{t0}}^{k_{t0}+N_{\text{et}}-1}|D_{\omega q}(k_t,k_x,k_y)|^2}{\sum_{k_t=k_{t0}-N_{et}}^{k_{t0}-1}|D_{\omega q}(k_t,k_x,k_y)|^2}-1\right). \tag{11}$$

Under the noise only hypothesis, $\mathcal{H}_{0e}$: both segments have the same PSD and then R_{et} can be modeled by a Gaussian random variable with zero mean and unitary variance. Under the signal plus noise hypothesis $\mathcal{H}_{1e}$: the evaluated point k_{t0} is located at a boundary, where the points at the right of k_{t0} have a PSD σ_r^2 greater than the PSD, σ_l^2 of the points at the left of k_{t0}, and $\gamma_e = \sigma_r^2/\sigma_l^2$, then R_{et} can be approximated by a Gaussian random variable with mean $\gamma_e\sqrt{N_{et}/2}$ and variance $(1+\gamma_e)^2$.

The probabilities of false alarm, P_{fet}, and the probability of detection, P_{det}, are obtained for a given threshold value λ in the following way

$$P_{fet} = \mathcal{Q}\left(\frac{\lambda-\mu_{He0}}{\sigma_{He0}}\right) = \mathcal{Q}(\lambda), \quad P_{det} = \mathcal{Q}\left(\frac{\lambda-\mu_{He1}}{\sigma_{He1}}\right), \tag{12}$$

where $\mathcal{Q}(\cdot)$ is the standard Gaussian complementary cumulative distribution function, and $[\mu_{He0}, \sigma_{He0}]$ and $[\mu_{He1}, \sigma_{He1}]$ are the mean and variance of R_k under the two evaluated hypotheses. It is worth to note that other possible scenarios, different to the two main hypotheses, are possible. As an instance, the case in which the PSD is not constant inside the evaluated segments, or even the simple case where γ_e is lower than one (falling edge case).

A more reliable test statistic can be obtained using multiple realizations of $D_{\omega q}(k_t,k_x,k_y)$ having in consideration that the boundaries in the subbands are remain unchanged even if the occupancy and PSD of each of the subbands are changed.

The consolidated test statistic can be obtained by averaging the absolute value of R_{et} as proposed in [7], or using a logical operator over multiple detection results given by single realizations.

For the detection of the edges in the angular dimension, we propose a similar procedure in which the length of the averaged segment in the k_x (or the k_y) is equal to one. Wherewith, the test statistic, for a given k_t, and k_y and for an evaluated point k_{x0} becomes

$$R_{ex}(k_{x0}) = \sqrt{\frac{1}{2}}\left(\frac{|D_{\omega q}(k_t, k_{x0}, k_y)|^2}{|D_{\omega q}(k_t, k_{x0}-1, k_y)|^2} - 1\right). \quad (13)$$

The probabilities of false alarm and detection can be found in a similar way to the one used in the k_t axis. After performing these procedures in the three axes, a set of volumetric sets are classified and used for its detection.

B. Generalized Energy Detection

After the samples $D_{\omega q}(k_t, k_x, k_y)$ are classified in different tridimensional subbands, the average energy is computed for each of these subbands. Having the assumption that there is always a white subband at any moment, the subband with the lowest average power is selected as white and used as the reference subband for the other subbands. The test statistic for each subband is obtained from the ratio between its average energy and the average energy of the reference subband. Let us assume that the reference subband has a length of N_{dt} in the k_t axis, N_{dx} in the k_x axis and N_{dy} in the k_y axis for a total of $N_d = N_{dt}N_{dx}N_{dy}$. Similarly, the sth evaluated tridimensional subband has a total number of points $N_s = N_{st}N_{sx}N_{sy}$.

For each subband, the average energy, Æ_s is computed by averaging $|D_{\omega q}(k_t, k_x, k_y)|^2$ for the points inside each subband, and the test statistics for the detection of the sth sub-band is computed by

$$R_s = \sqrt{\frac{N_d N_s}{N_d + N_s}}\left(\frac{\text{Æ}_s}{\text{Æ}_d} - 1\right), \quad (14)$$

where Æ_s is the average energy in the sth evaluated subband and Æ_d is the average energy in the reference subband. It can be shown that R_s is a Gaussian random variable with mean $\gamma_s\sqrt{N_d N_s/(N_d+N_s)}$ and variance $(1+\gamma_s)^2$, where $\gamma_k \geq 0$ is the SNR of sub-band s (i.e., $\gamma_s = 0$ under noise only case). The probabilities of false alarm, P_f, and the probability of detection, P_d, are obtained for a given threshold value λ as [7]

$$P_f = \mathcal{Q}\left(\frac{\lambda - \mu_{H0}}{\sigma_{H0}}\right) = \mathcal{Q}(\lambda), \quad P_d = \mathcal{Q}\left(\frac{\lambda - \mu_{H1}}{\sigma_{H1}}\right). \quad (15)$$

where $\mathcal{Q}(\cdot)$ is the standard Gaussian complementary CDF, and $[\mu_{H0}, \sigma_{H0}]$ and $[\mu_{H1}, \sigma_{H1}]$ are the mean and variance of R_s under the two possible hypothesis, $\mathcal{H}_0$: the sensed sub-band is free and $\mathcal{H}_1$: the sensed sub-band is occupied.

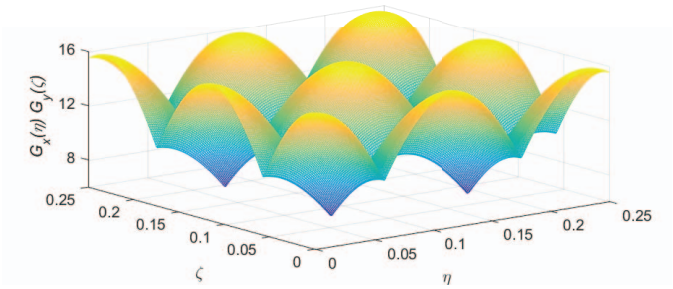

Fig. 3. $|G_x G_y(\eta, \zeta)|$ for the case $N_x = N_y = 16$. The maximum amplitude gain is $\sqrt{N_x N_y} = 16$

IV. System Analysis and Simulation Results

In order to validate the proposed technique, we simulate the system using different number of antennas separated by one half of the carrier wavelength. The array is tested using different number of incident wavefronts with different incident angles and power flux densities. An incident wavefront with power flux density Φ_0 inside a given subband will produce a given PSD inside the given subband for the given the array gain, as explained in the following subsection.

A. Array gain

The maximum array gain is obtained when the angular frequencies η and ζ of the incident wavefront are integer multiples of $1/N_x$ and $1/N_y$. In this case, all the energy remains concentrated in one $[k_{x0}, k_{y0}]$ pair of values inside the matrix $D_\omega(k_t, k_x, k_y)$, and no contribution is seen for the points with $k_x \neq k_{x0}$, $k_y \neq k_{y0}$. Consequently, the amplitude gain in the peak will be $\sqrt{N_x N_y}$ and therefore the power gain becomes $N_x N_y$. This maximum gain is not observed for all the incident angles, and the actual value is obtained from the projection of η and ζ in the summation of (7). It can be seen that this gain is a periodic function of the incident angle that varies between 1 and $2/\pi$. As an instance, for the cases in which N_x (and similarly for N_y) is an integer multiple of 4, the gain in amplitude can be approximated by

$$G_x(\eta) = \sqrt{N_x}\left(\left|\cos\left(\eta\frac{\pi N_x^2}{2(N_x-1)}\right)\right|\left(\frac{2-\pi}{\pi}\right) + \frac{2}{\pi}\right). \quad (16)$$

Using $G_x(\eta)$ and $G_y(\zeta)$, the array gain in amplitude will be $G_x(\eta)G_y(\zeta)$. Figure 3 shows an example of the array gain for the particular values of number of rows and columns of antennas, $N_x = N_y = 16$, for the values of η and ζ from 0 to 0.25.

B. Quantization effects

For evaluating the quantization effect, a set of Monte-Carlo simulations were performed using one-bit quantization, for different numbers of incident wavefronts, and for different number of antennas. For the simulations, we assume omni-directional receivers at ambient temperature (300K) and 6dB noise figure, separated by half wavelengths in the x and y axes. We take 256 temporal samples in each antenna at a sampling

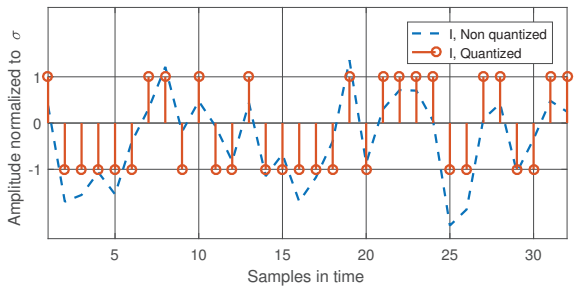

Fig. 4. One-bit quantization of the baseband received signal. The one-bit ADC is a zero crossing comparator for the I and Q baseband components.

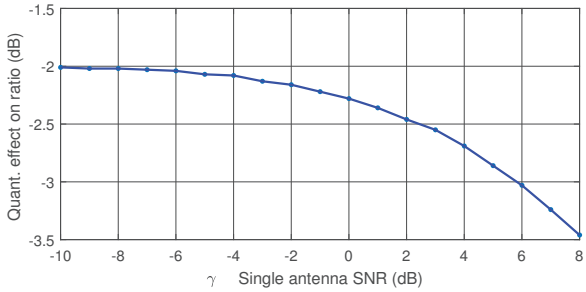

Fig. 5. Ratio in dB of the test statistics obtained from a one-bit quantized signal to the non quantized test statistics. This is plotted as a function of the single antenna SNR γ.

frequency of 40MHz which represents a sensing time of 6.4 μsecs. We simulate two simultaneous incident wavefronts with two arbitrarily selected incident angular frequencies, one at $[\eta,\zeta] = [0.4, 0.4]$ and another one at $[\eta,\zeta] = [0.11, -0.7]$. The total bandwidth was divided in 8 subbands with the same size. The energy of the incident wavefronts were only allocated in one of these subbands. To obtain this behavior, an OFDM was implemented using two type of symbols, first, a QPSK constellation with random symbols or second a set of random complex numbers (with random angle and amplitude), and then we vary the incident power flux density to obtain different SNR values for a single antenna. One-bit quantization is performed for each of the I and Q components of the received signal. Figure 4 shows an snapshot of a section of the received signal, in which the sign of the I component is quantized.

We compute the ratio R_s for both cases, the quantized and non quantized matrices, assuming that we know a priori the location of the evaluated subbands which includes a single value for k_x, k_y. For the reference subband, we use a range of indexes in order to get an average that includes a set of tri-dimensional points. We compute this test statistic for the simulated data using the quantized and not quantized version of the received signals, and in this way get the test statistics from $D_{\omega q}(k_t, k_x, k_y)$ and $D_{\omega}(k_t, k_x, k_y)$ respectively. We computed the ratio of these two test statistic using 2^{20} realizations whose results are in Figure 5 for $N_x = N_y = 16$. From here we corroborate the limit of $2/\pi$ (-1.96dB) degradation in the mean of the test statistics for the quantized version. From Figure 5, it can be seen that the degradation can be tractable (around 2.5dB) for medium SNR values around 3dB.

C. Subband detection

We also performed Monte-Carlo simulations to corroborate the theoretical expressions for P_d and P_f obtained for the proposed detector including the $2/\pi$ correction for the quantization effect. We checked the P_f values for other indexes different to the ones occupied by the PU incident wavefronts, and we ensured that it follows accurately the analytical equation as a function of the threshold. Next, we checked the P_d from the simulated data and checked concordance with the theory. Figure 6 shows a plot of P_d versus P_f for different SNR values. In this point, we also show in Figure 7 the analytical curves for the required sensing time for the worst case of the array gain.

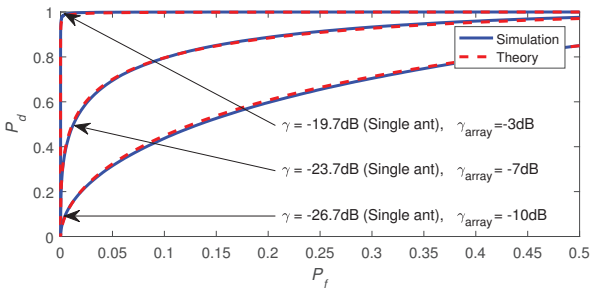

Fig. 6. Simulation results for P_d as a function of P_f. The plots are obtained using 1024 samples in time, equivalent at 40MHz to 25.56μsecs (N_s = 1024 and N_d =65536). The array gain with the especific $\eta, \zeta = 0.4, 0.4$ is 18.72 dB. Finally the γ_{array} is affected by quantization degradation which is -1.96dB.

D. Power consumption and system complexity

The power consumption of the proposed signal is evaluated in relation to a single antenna full resolution ADC receiver. For the conventional flash ADC, it is stated that the size and power consumption doubles for the increase of one bit in the resolution [10], [21]. The power consumption of a dual ADC (I and Q branches) with a resolution of b bits, working at a sampling frequency of F_s can be approximated to $2^{b+1} F_s K_{\text{tech}}$, where

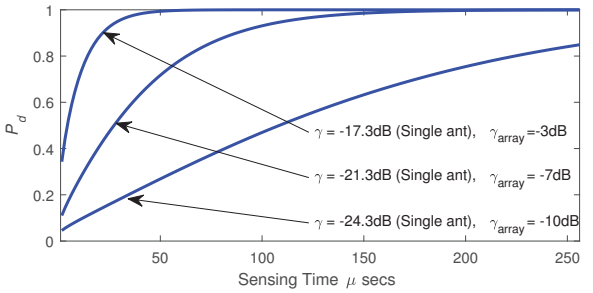

Fig. 7. Analytical values for P_d as a function of the sensing time (N_s/N_d= 1024/65536). The especific $\eta, \zeta = 0.4102, 0.4102$ which is one of the worst degradation possible for $G_x(\eta)G_y(\zeta)$ which is 16.24dB. Finally the γ_{array} is affected by quantization degradation which is -1.96dB.

K_{tech} is a parameter given by the implementation technology used. In contrast to this, the consumption of the one-bit ADC will be the one of a single comparator per branch, which can be accomplished with a few transistors, and will have a power consumption of $2^{1+1}F_sK_{\text{tech}}$ [21]. In this case, the power consumption of a dual 16 bits ADC will be the same of the all ADCs in an array with with 65536 antennas, which is two orders of magnitude higher than the number of antennas evaluated on the simulations. For the analog front-end part, it is also observed that some improvement can be obtained due to the dynamic range of the input signal which is substantially reduced. This reduction gives the possibility to perform a single stage analog processing without the need to perform an Automatic Gain Controllled (AGC) amplifier.

V. Conclusions

This paper has proposed a novel spatio-temporal wideband spectrum sensing technique which is based on a multi-antenna receiver with one-bit complex quantization. It has been shown that the proposed spectrum sensing technique can improve the detection performance, in terms of detection statistics for a given incident power and sensing times, while decreasing the total consumed power and system complexity compared to the single-antenna high-resolution ADC case.

The proposed method was verified by simulations for different parameter settings. Furthermore, it has been illustrated that the proposed method can obtain the desired detection performance with a sensing time which is several order of magnitudes lower than the conventional case. In addition, this reduction can help to alleviate the non-ergodicity effects over the GED under the assumption that all the receiver chains in the array have the same noise distribution. This is a reasonable assumption since the detector can be designed as a compact device in which all the antennas and receive chains employ the same physical parameters. In addition, the proposed technique provides spatial information for the detected PUs, which can improve the overall CRN performance while providing better protection to the PUs.

Acknowledgements

This work was partially supported by National Research Fund, Luxembourg under CORE projects “SeMIGod” and “SATSENT”.

References

[1] *et al* J. G. Andrews, “What will 5G be?,” *IEEE Journal on Selected Areas in Communications*, vol. 32, no. 6, pp. 1065–1082, June 2014.

[2] *et al* R. H. Tehrani, “Licensed spectrum sharing schemes for mobile operators: A survey and outlook,” *IEEE Commun. Surveys Tutorials*, vol. PP, no. 99, pp. 1–1, 2016.

[3] J. Mitola and G. Q. Maguire, “Cognitive radio: making software radios more personal,” *IEEE Personal Communications*, vol. 6, no. 4, pp. 13–18, Aug 1999.

[4] S. K. Sharma, T. E. Bogale, S. Chatzinotas, B. Ottersten, L. B. Le, and X. Wang, “Cognitive radio techniques under practical imperfections: A survey,” *IEEE Communications Surveys Tutorials*, vol. 17, no. 4, pp. 1858–1884, Fourthquarter 2015.

[5] R. Tandra and A. Sahai, “SNR walls for signal detection,” *IEEE J. Sel. Topics Signal Process.*, vol. 2, no. 1, pp. 4 – 17, Feb. 2008.

[6] D. Cabric, S.M. Mishra, and R.W. Brodersen, “Implementation issues in spectrum sensing for cognitive radios,” in *Conference Record of the Thirty-Eighth Asilomar Conference on Signals, Systems and Computers*, 2004, vol. 1, pp. 772–776 Vol.1.

[7] T. E. Bogale, L. Vandendorpe, and L. B. Le, “Wideband sensing and optimization for cognitive radio networks with noise variance uncertainty,” *IEEE Trans. Commun.*, vol. 63, no. 4, pp. 1091–1105, April 2015.

[8] J. C. Merlano-Duncan, T. E. Bogale, and L. B. Le, “SDR implementation of spectrum sensing for wideband cognitive radio,” in *IEEE 82nd Vehicular Technology Conference (VTC Fall)*, Sept 2015, pp. 1–5.

[9] T. E. Bogale and L. B. Le, “Massive MIMO and mmWave for 5G wireless hetnet: Potential benefits and challenges,” *IEEE Vehicular Technology Magazine*, vol. 11, no. 1, pp. 64–75, March 2016.

[10] Seyed Alireza Zahrai and M. Onabajo, “A low-power hybrid ADC architecture for high-speed medium-resolution applications,” in *IEEE 58th International Midwest Symposium on Circuits and Systems (MWSCAS)*, Aug 2015, pp. 1–4.

[11] J. Mo and R. W. Heath, “Capacity analysis of one-bit quantized MIMO systems with transmitter channel state information,” *IEEE Transactions on Signal Processing*, vol. 63, no. 20, pp. 5498–5512, Oct 2015.

[12] A. Mezghani and J. A. Nossek, “On ultra-wideband MIMO systems with 1-bit quantized outputs: Performance analysis and input optimization,” in *2007 IEEE International Symposium on Information Theory*, June 2007, pp. 1286–1289.

[13] A. Ali and W. Hamouda, “Low power wideband sensing for one-bit quantized cognitive radio systems,” *IEEE Wireless Communications Letters*, vol. 5, no. 1, pp. 16–19, Feb 2016.

[14] O. Mehanna and N. D. Sidiropoulos, “Frugal sensing: Wideband power spectrum sensing from few bits,” *IEEE Transactions on Signal Processing*, vol. 61, no. 10, pp. 2693–2703, May 2013.

[15] O. Mehanna and N. D. Sidiropoulos, “Maximum likelihood passive and active sensing of wideband power spectra from few bits,” *IEEE Transactions on Signal Processing*, vol. 63, no. 6, pp. 1391–1403, March 2015.

[16] M. Nekovee, T. Irnich, and J. Karlsson, “Worldwide trends in regulation of secondary access to white spaces using cognitive radio,” *IEEE Wireless Communications*, vol. 19, no. 4, pp. 32–40, August 2012.

[17] ECC Report 159, “Technical and operational requirements for the possible operation of cognitive radio systems in the white spaces of the frequency band 470-790 mhz,” Tech. Rep., CEPT SE43 Working Group, 2011.

[18] C. S. Ruf, C. T. Swift, A. B. Tanner, and D. M. Le Vine, “Interferometric synthetic aperture microwave radiometry for the remote sensing of the earth,” *IEEE Transactions on Geoscience and Remote Sensing*, vol. 26, no. 5, pp. 597–611, Sep 1988.

[19] P. J. Napier, A. R. Thompson, and R. D. Ekers, “The very large array: Design and performance of a modern synthesis radio telescope,” *Proceedings of the IEEE*, vol. 71, no. 11, pp. 1295–1320, Nov 1983.

[20] A. Camps, J. Bara, I. C. Sanahuja, and F. Torres, “The processing of hexagonally sampled signals with standard rectangular techniques: application to 2-d large aperture synthesis interferometric radiometers,” *IEEE Transactions on Geoscience and Remote Sensing*, vol. 35, no. 1, pp. 183–190, Jan 1997.

[21] A. Khorami, M. B. Dastjerdi, and A. F. Ahmadi, “A low-power high-speed comparator for analog to digital converters,” in *2016 IEEE International Symposium on Circuits and Systems (ISCAS)*, May 2016, pp. 2010–2013.